International Journal of Mass Spectrometry 304 (2011) 57–65

Contents lists available at ScienceDirect

International Journal of Mass Spectrometry

journal homepage: www.elsevier.com/locate/ijms

Ionic and vibrational properties of an ultra-low ionization potential molecule: Tetrakis(dimethylamino)ethylene

Nasrin Mirsaleh-Kohan[a,b,*], Wesley D. Robertson[a,c], Jason Lambert[a], R.N. Compton[a,b], Serge A. Krasnokutski[d], Dong-Sheng Yang[d]

[a] Department of Physics, The University of Tennessee, Knoxville, TN 37996, United States
[b] Department of Chemistry, The University of Tennessee, Knoxville, TN 37996, United States
[c] Department of Physics, Emory University, Atlanta, GA 30322, United States
[d] Department of Chemistry, University of Kentucky, Lexington, KY 4056, United States

ARTICLE INFO

Article history:
Received 4 November 2010
Received in revised form 8 April 2011
Accepted 8 April 2011
Available online 15 April 2011

Keywords:
Tetrakis(dimethylamino)ethylene
Low ionization potential
Electron and photon ionization
Raman frequencies
Trochoidal electron monochromator (TEM)
Nozzle-jet expansion

ABSTRACT

Threshold ionization spectra of nozzle-jet cooled tetrakis(dimethylamino)ethylene (TDAE) were measured with high-resolution electron and laser ionization techniques, and Raman spectra of the molecule at room temperature and under liquid nitrogen were recorded with laser excitation. The TDAE ion signal shows a gradual increase at the onset of ionization, and the upper bounds of the adiabatic ionization potential (IP) measured from the electron ionization and laser ionization are 5.3 ± 0.2 and 5.20 ± 0.05 eV, respectively. In combination with the experimental measurements, density functional theory calculations were used to predict the adiabatic and vertical IPs and vibrational frequencies. The predicted adiabatic IP (5.2 eV) and C=C stretching frequency (1622 cm^{-1}) are in excellent agreement with the measured values. The adiabatic IP is about 0.6 eV lower than the vertical IP (5.8 eV). The large difference between the adiabatic and vertical IPs arise from the significant geometry change upon ionization and is consistent with the experimental observation of the slowly rising ion signal at the ionization onset of the molecule in both the electron ionization and photoionization experiments. Raman spectroscopy of TDAE at room temperature and at liquid nitrogen (Raman under nitrogen, RUN) is reported in an attempt at examining higher energy conformers.

1. Introduction

The ionization potential (IP) of most organic compounds lies in the range from 7 to 12 eV. However, a previous photoionization study indicated that tetrakis(dimethylamino)ethylene ($C_{10}H_{24}N_4$, TDAE) has a very low IP ($\leq$5.36 eV) [1], which is comparable to that of the lithium atom (5.39 eV). Such a low IP molecule has attracted great interest over the past decade. Since TDAE readily gives up an electron, it has found many applications in various applied and research areas, such as plasma technology, semi-conductor industry, and electrospray mass spectrometry.

In plasma research, a central interest is on the study of high-density, low-temperature plasmas (about 10^{11-13} cm^{-3}) at atmospheric pressure. The main difficulty of producing these plasmas is a requirement of high power budget to initiate and sustain an air-plasma discharge. The high power budget can be reduced to some extent by the choice of a seed gas. Woodworth et al. [2] studied the generation of a high-density plasma by using ultraviolet (UV) lasers to ionize low IP organic molecules. Scharer's group [3,4] successfully produced plasmas with densities of about 10^{13} cm^{-3} in TDAE vapor through a 193 nm one-photon ionization process.

TDAE has also found important applications in particle physics and medical imaging. An alternative to expensive photomultiplier tubes in detecting UV photons is to employ photosensitive gases [5,6]. Detectors based on photosensitive gases can be employed to detect UV photons over large areas with a reasonable cost. In designing a detector based on these photosensitive gases, the absorption photon wavelength and absolute quantum efficiency are two important parameters. TDAE with its high vapor pressure (0.35 Torr at 20 °C), large quantum efficiency, and broad spectrum of sensitivity has proved to be an ideal gas for the detection of UV photons [7]. Another interest in TDAE arises from its ferromagnetic properties when it is doped into fullerene crystals, i.e., TDAE-C_{60}. In 1991, Allemand et al. [8] recognized for the first time that TDAE-C_{60} is a ferromagnetic material with a Curie transition temperature of 16 K. Later, Tanaka et al. [9] reported three magnetic phases for TDAE-C_{60} with Curie transition temperature of 25, 16, and 10 K. TDAE also has been chosen to reduce the barrier for the charge injection in electronic devices. It has been shown that a monolayer of TDAE deposited on a gold

* Corresponding author.
E-mail address: nmirsale@utk.edu (N. Mirsaleh-Kohan).

1387-3806/$ – see front matter © 2011 Elsevier B.V. All rights reserved.
doi:10.1016/j.ijms.2011.04.002

substrate decreases the work function of the surface by 1.3 eV [10].

Furthermore, TDAE is making an impact on the emerging field of multiply-charged anions. One of the challenges in studies of multiply-charged anions (MCA) is the production of MCA in the gas phase. Although, the development of the electrospray ionization source [11] has revolutionized the process of producing MCA, for species such as fullerenes, generating doubly charged anions still remains a difficult task. Interestingly, adding TDAE as a strong electron donor to the fullerene solution before spraying into the electrospray ionization source generally assists in the production of doubly-charged anions of fullerenes. In this context, Hampe et al. [12] produced doubly charged of C_n^{2-} where $n = 74$ and 78–124 upon adding 2 mol of TDAE to a 1 mM fullerene solution. The $C_{60}F_{34}^{2-}$ and $C_{60}F_{46}^{2-}$ ion signals were also greatly enhanced using TDAE as an electron donor [13].

When Pruett et al. [14] were first synthesizing TDAE in 1950; they observed the emission of green chemiluminescence when TDAE was in contact with air. This observation was an unexpected behavior for such ethylene type derivatives. Later, this was explained by noting that since TDAE is an exceptionally electron rich alkene it could be oxidized very easily. This property of TDAE can be effectively used in the detection of oxygen. In addition to the synthetic method used by Pruett et al. [14], a few other methods have been successfully used in the preparation of TDAE [15,16].

The reactivity of an organic compound with at least one carbon–carbon double bond (C=C) is strongly influenced by the substituents attached to the carbons. If the substituents withdraw the electrons from the carbon–carbon double bond, then the organic compound is an electron acceptor. However, if the substituents attached to the carbon atoms increase the electron density around the carbon–carbon bond, this compound can be an electron donor. TDAE has four amino groups attached to the two central ethylenic carbon atoms and is an example of a strong electron donor in many reactions. Wiberg [17] attributed the readiness of TDAE to give up electrons to the presence of the four amino groups. The amino groups stabilize the positive ions of TDAE by partially transferring their free electron pairs to the central carbon atoms (C=C). The chemical properties of TDAE have been discussed extensively in Wiberg's review article [17].

Nakato et al. [1] reported the first gas-phase IP of TDAE in 1971. They obtained an adiabatic IP of ≤5.36 eV and a vertical IP of 6.11 eV for TDAE at room temperature by using a hydrogen-discharge lamp with the photon bandwidth of 0.02 eV. These IP values were estimated by measuring the photoelectron current as a function of photon energy. The accurate measurement of the adiabatic IP was difficult since the onset of ionization was rather gradual. In addition, the sample was held at room temperature making possible "hot band" effects in the ionization threshold. A He(I) photoelectron experiment performed by Centinkaya et al. [18] reported a value of 5.95 eV for the vertical IP of TDAE. This experiment also involved TDAE at room temperature.

There are also a few theoretical studies of adiabatic and vertical ionization potentials of TDAE. A study by Martin et al. [19] reported values of 4.95 and 5.62 eV for the adiabatic and vertical IPs, respectively. Pederson and Laouini [20] reported two values for vertical IP: 5.88 eV by including spin polarization effects and 5.80 eV without considering the spin polarization. Moreover, they further calculated the highest occupied molecular orbital (HOMO) of the TDAE in order to identify its donor electron. These authors reported that the donor electron is mostly delocalized over the C=C bond and the neighboring four N atoms, i.e., interior part of the molecule. They concluded that the TDAE molecule donates an electron with little change in its molecular size.

Although there have been extensive studies describing TDAE as an electron donor, its molecular conformation is not well characterized. Gas-phase electron diffraction studies [21] show that TDAE is composed of four identical $N(CH_3)_2$ groups attached to the C=C double bond. The repulsion between the four amino groups in TDAE prevents the formation of a planar structure for TDAE. A Raman spectrum showed [22] a very intense band in the C=C region ($1630\,cm^{-1}$), whereas this mode exhibits no infrared absorption [23]. This mutual exclusion indicated that the TDAE is symmetric about the C=C region, but it gives no information about the arrangement of the dimethylamino groups. A study by Wiberg [17] concluded that since the energy barrier for the rotation of the dimethylamino groups about the C–N bond is very small, they can rapidly rotate about the C–N bond giving TDAE several rotational isomers. A study by Bock et al. [21] employing gas-phase electron diffraction revealed some structural information on TDAE. They determined that the two molecular halves $[N_2(CH_3)_2]$ on both sides of the C=C axis are twisted relative to each other by 28°. The bond distances were reported to be 1.36, 1.40, and 1.45 Å for C=C, C–N, and N–CH_3, respectively.

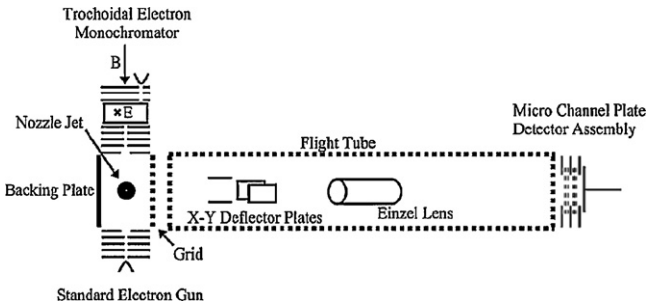

Fig. 1. A schematic diagram of the linear electron ionization time-of-flight mass spectrometer. The low-resolution standard electron gun and high-resolution trochoidal electron monochromator are located on opposite sides of the ionization region. In the drift region, a set of X–Y deflectors and a cylindrical Einzel lens are used to focus the ions beam [24].

In this work, we report the adiabatic IP values of the nozzle-jet expanded (ro-vibrationally cooled) TDAE measured from electron ionization (EI) and laser photoionization (PI) spectra, a C=C stretching frequency from argon ion laser (514.5 nm) excitation Raman spectra, and molecular fragmentation from EI ionization time-of-flight mass spectra. Moreover, we present molecular geometries, adiabatic and vertical IPs, and vibrational frequencies of the TDAE molecule from Becke's 3-parameter hybrid density functional theory (DFT/B3LYP) calculations. From the experimental measurements and theoretical calculations, we find relatively large structural changes of TDAE upon ionization.

2. Materials

Tetrakis(dimethylamino)ethylene ($C_{10}H_{24}N_4$, TDAE) was purchased from Sigma–Aldrich stored at low temperature and used with no further purification. Due to the air sensitivity of this compound, sample preparation was performed using an argon-purged glove bag.

3. Experimental methods

3.1. Electron ionization experiment

A linear time-of-flight mass spectrometer (TOFMS) was employed to record the mass spectra and adiabatic IP of TDAE. In this system (Fig. 1), which has been described previously [24], electron ionization is used as the source of ionization [25]. The electrons are generated by one or both of the two electron guns, a low-resolution standard electron gun or a high-resolution trochoidal electron monochroma-

tor (TEM) [26] is used to generate high-resolution electron beams. A typical TEM produces a tunable monoenergetic electron beam with intensities on the order of nanoamperes and an electron energy resolution of 0.1–0.02 eV. In the present TOFMS, molecules are introduced into the interaction region via a seeded nozzle jet that provides a rotationally, vibrationally, and translationally cooled molecular beam. This molecular beam is crossed at right angles with the beam of energy-selected electrons in the interaction region. The Wiley–McLaren [27] space-focusing condition is used to increase the time-of-flight mass resolution of the ion beam. The entire system is pumped by two 300 l/min roughing pumps (Varian) separately in line with two 550 l/s turbomolecular pumps. The base pressure of the TOFMS is $\sim 10^{-9}$ Torr.

The TDAE vapor was introduced across the electron beam through a nozzle-jet with argon gas at backing pressures of an atmosphere. The extent of ro-vibrational cooling is unknown but believed to be significant. The electrons were produced by one of the electron guns discussed above depending on the required energy resolution and intensity of the electron beam in the study. The molecules that do not interact with the electron beam are pumped out of the chamber. Mass spectra of the TDAE ions were obtained using the standard electron gun (10^{-5} A) in order to produce sufficient ion signals. A Hewlett-Packard digital oscilloscope (Infinium 500 MHz) was used to view the time-of-flight spectrum. Grams^{TM} software was used to convert the time scale to the mass scale spectrum using known mass peaks such as Xe and Ar for the calibration. The IP of the parent ion was recorded employing the TEM electron gun. The resolution of the TEM was set to approximately 0.1 eV. In order to record a mass signal versus electron energy, a mass peak was selected and averaged by using a Stanford Research Systems box integrator (SR 250). A Labview^{TM} computer program was also used to collect the data from the Boxcar Integrator in order to plot the intensity of a chosen peak versus electron energy. The argon carrier gas (IP = 15.75 eV) was used to calibrate the electron energy scale.

3.2. Photoionization experiment

Photoionization measurements were carried out with an experimental setup described in a previous publication [28]. The setup consists of two vacuum chambers: the first chamber contains a supersonic molecular beam source, and the second chamber houses a homemade, two-field, time-of-flight mass spectrometer. TDAE was introduced at room temperature and seeded in ultra high purity He or Ar gas (Scott-Gross) at 50 psi. The mixture of the inert gas and organic vapor was then supersonically expanded to the source vacuum chamber through a general valve (series 9) operated in a 10 Hz pulsed mode. Mass spectra were measured by photoionization time-of-flight mass spectrometry, and photoionization efficiency spectra were obtained by recording the mass-selected ion signal as a function of the laser wavelength. Ionization was carried out by a frequency-doubled dye laser (Lumonics, HD-500), pumped by the third harmonic output (355 nm) of a Nd:YAG laser (Quanta-Ray, GCR-3). The ion signal was detected by a dual micro-channel-plate detector (Galileo), amplified by a preamplifier (Stanford Research System SR445), averaged by a gated integrator (Stanford Research System SR250), and recorded in a laboratory computer.

3.3. Raman experiment

The Raman spectra were recorded with a Dilor XY-800 confocal micro-Raman spectrometer [29]. Laser excitation was obtained using a 100 mW Lexel, Inc, 3500 argon ion laser (514.5 nm). Due to the air sensitivity of TDAE, the sample was placed in a sealed glass tube. The experiment was performed at room temperature (20 °C).

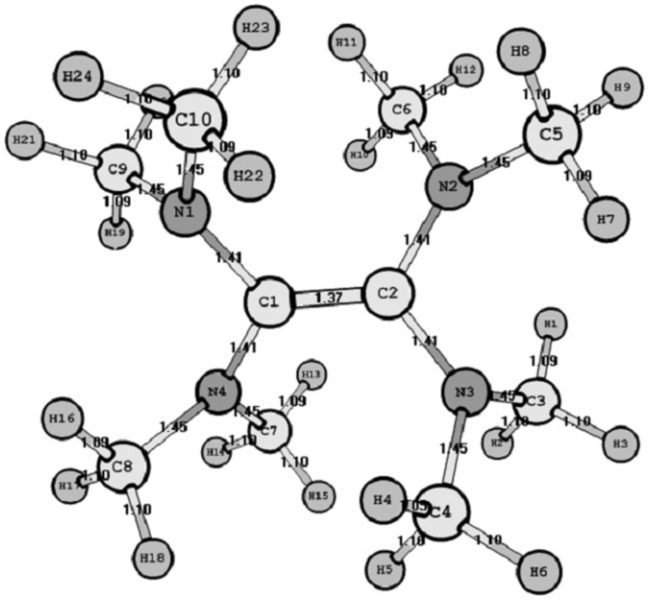

Fig. 2. Computed D_2 structure and bond lengths of neutral TDAE. All bond lengths are in angstroms.

The laser light was focused on the sealed sample through a 80× objective of the microscope. Raman spectrum for TDAE under liquid nitrogen (RUN) was also recorded in order to obtain a higher resolution Raman spectrum as well as obtaining information regarding the presence of conformers of TDAE [29]. In this regard, the sealed sample was placed under liquid nitrogen and the laser beam was passed through the liquid nitrogen and the glass. The Raman experiment under liquid nitrogen condition provided more information about the Raman bands and will be discussed in Section 5. RUN spectroscopy has been shown to provide ro-vibrational cooling of the sample as well as the quenching of higher energy molecular conformers. RUN spectrum often exhibits less fluorescence background.

4. Computational methods

Geometry optimizations of neutral and positively charged TDAE ($C_{10}H_{24}N_4$) were performed using DFT/B3LYP method (B3LYP) and 6-311++G (d,p) and 6-311+G(d,p) basis sets. All calculations were performed using the Gaussian 03 program suite [30].

Vibrational frequencies of the neutral and singly charged positive ion of TDAE were also computed for several reasons. First, to confirm that the optimized geometry is a minimum energy structure, which should have no negative (imaginary) frequencies. Second, to obtain the zero-point energy needed to calculate the adiabatic IP of TDAE. Finally, the calculated vibrational frequencies will be compared to the experimental Raman spectra to further assess the accuracy of the calculations.

5. Results and discussion

5.1. Computational results

The computed molecular structure of the lowest energy neutral TDAE is presented in Fig. 2. The TDAE structure was found to be a non-planar structure with D_2 symmetry. As shown in Fig. 2, the C=C, C–N, N–CH_3, and C–H bond distance was found to be 1.37, 1.41, and 1.45, 1.1 Å, respectively, for the neutral TDAE. The distances obtained from the calculations are in good agreement with the data reported from the gas-phase electron diffraction studies

Table 1
Computed values for adiabatic (IP_a) and vertical (IP_v) ionization potentials of TDAE. All values are in eV.

Computational method	IP_a (eV)	IP_v (eV)	Reference
B3LYP/6-311++G(d,p)	5.15	5.83	This work
B3LYP/6-311+G(d,p)	5.16	5.72	This work
B3LYP/4-21G	4.65	5.28	[19]
B3LYP/cc-pVDZ	4.95	5.62	[19]
Density functional (spin unpolarized)	–	5.80	[20]
Density functional (spin polarized)	–	5.88	[20]

Table 2
Experimental values for adiabatic (IP_a) and vertical (IP_v) ionization potentials of TDAE. All values are in eV.

Experimental method	IP_a (eV)	IP_v (eV)	Reference
Electron ionization	5.3 ± 0.2	–	This work
Photoionization	5.20 ± 0.05	–	This work
Photoionization	$\leq 5.36 \pm 0.02$	6.11 ± 0.02	[1]
Photoionization	–	5.95	[18]

[21]. Angles for N_1–C_1–N_4, C_9–N_1–C_{10}, N_1–C_1–C_2, and C_{10}–N_1–C_1 are also computed to be 113°, 116°, 124°, and 120°, respectively (see Fig. 1 for the notation).

For the singly charged TDAE, the C=C, C–N, N–CH_3 and C–H bond lengths are 1.43, 1.37, and 1.46, and 1.1 Å. The C=C bond distance increases significantly upon ionization, whereas the C–N bond length decreases. The N–CH_3 and C–H bond distances remain almost unchanged. Angles for N_1–C_1–N_4, C_9–N_1–C_{10}, N_1–C_1–C_2, and C_{10}–N_1–C_1 are also computed to be 118°, 115°, 121°, and 122°, respectively. One significant difference between the neutral and positive ion structures is the rotation of methyl groups. For example, the torsion angle C_2–N_2–C_6–H_{10} (Fig. 2) changes from 30° to 9° upon ionization. Because of these bond lengths and angle changes, the relative nuclear positions alternate considerably upon ionization. This contributes to the significant difference between adiabatic and vertical IPs.

Calculated and experimental vertical and adiabatic IPs for TDAE are shown in Tables 1 and 2. The adiabatic (vertical) IPs from the B3LYP/6-311++G(d,p) and B3LYP/6-311+G(d,p) calculations are 5.15 eV (5.83 eV) and 5.16 eV (5.72 eV), respectively. The difference between the adiabatic and vertical IPs is on the order of ~0.6 eV, which is another indication of structural change of TDAE upon ionization.

Computed vibrational frequencies and their Raman and IR intensities are listed in Tables 3 and 4 for the neutral molecule and the singly charged positive ion of TDAE. Since for both basis sets the calculated frequencies are in close agreement, only the results from one basis set (6-311++G(d,p)) are presented. The values of computed frequencies are scaled by a factor of 0.98 due to known systematic errors in the calculated frequencies [31].

According to the calculations, there is a very intense vibrational feature in the neutral TDAE that is attributed to the symmetric stretching mode of the central C_1=C_2 (1622 cm^{-1}). This mode is Raman active, but shows almost no IR activity. The 1622 cm^{-1} mode is also very well separated from other modes, making it easy to be identified experimentally. Calculation of the vibrational frequencies of the positive ion shows that the C=C stretching mode shifts to 1544 cm^{-1} upon ionization of TDAE. This frequency shift indicates a weakening C=C bond and is consistent with the predicted bond length increase from the neutral molecule to the ion.

Table 3
Computed vibrational frequencies (scaled by 0.98) and Raman (IR) intensities for neutral TDAE using B3LYP/6-311++G(d,p). Frequencies are in cm^{-1}, Raman activities are in $Å^4$/amu, and IR activities are in km/mol. The intense C=C stretch mode (1622 cm^{-1}) is highlighted.

Mode ν_n	Frequency	Raman (IR) activity	Mode ν_n	Frequency	Raman (IR) activity	Mode ν_n	Frequency	Raman (IR) activity
1	65.8	1.0 (2.3)	37	1032.6	0.8 (199.6)	73	1456.2	5.7 (2.2)
2	66.4	0.6 (0.0)	38	1047.5	4.3 (2.6)	74	1462.1	0.6 (15.0)
3	76.7	0.3 (0.0)	39	1047.8	7.0 (8.0)	75	1465.8	5.7 (5.0)
4	80.8	0.1(0.6)	40	1050.2	4.8 (5.0)	76	1467.6	0.9 (19.2)
5	102.0	3.3 (0.6)	41	1050.4	2.7 (10.1)	77	1467.8	4.4 (0.9)
6	125.1	0.4 (2.5)	42	1081.6	0.6 (191.4)	78	1476.9	2.5 (13.1)
7	126.2	2.4 (0.1)	43	1091.3	0.6 (0.4)	79	1477.5	2.8 (10.3)
8	131.3	1.2 (1.3)	44	1093.7	0.8 (23.9)	80	1485.3	20.2 (0.6)
9	162.1	0.1 (3.2)	45	1095.3	1.2 (1.9)	81	1487.8	0.0 (27.3)
10	174.9	0.8 (1.1)	46	1097.3	6.6 (6.1)	82	1495.9	8.3 (28.8)
11	177.0	1.8 (0.1)	47	1119.2	9.7 (0.0)	83	1498.0	34.3 (6.2)
12	185.8	0.9 (0.6)	48	1134.5	0.2 (9.8)	84	1622.0	347.5 (1.5)
13	188.4	1.5 (0.5)	49	1136.3	10.2 (3.0)	85	2849.7	210.8 (102.5)
14	204.9	1.5 (0.0)	50	1138.9	0.6 (17.6)	86	2851.1	279.0 (167.0)
15	217.9	0.1 (2.2)	51	1142.1	2.8 (3.2)	87	2872.4	133.2 (107.2)
16	230.9	0.3 (2.5)	52	1213.3	0.9 (11.5)	88	2873.8	180.5 (120.8)
17	237.0	0.7 (0.0)	53	1219.3	3.0 (0.0)	89	2879.1	5.2 (281.4)
18	243.7	1.0 (1.7)	54	1226.7	8.5 (46.4)	90	2880.0	491.7 (5.1)
19	261.2	3.9 (3.0)	55	1235.0	0.2 (60.8)	91	2907.8	6.4 (185.3)
20	296.9	0.7 (9.6)	56	1288.5	1.3 (0.5)	92	2909.1	284.3 (1.2)
21	313.2	7.8 (0.0)	57	1315.4	1.3 (109.5)	93	2954.8	17.7 (110.9)
22	323.9	4.7 (2.1)	58	1330.6	0.5 (184.1)	94	2955.0	204.3 (6.7)
23	337.9	0.8 (13.8)	59	1340.0	14.9 (18.9)	95	2964.0	36.2 (102.1)
24	354.7	0.6 (1.6)	60	1407.1	6.3 (0.2)	96	2964.2	291.4 (18.6)
25	358.2	0.5 (0.7)	61	1408.1	9.0 (1.0)	97	2968.6	96.0 (66.2)
26	411.8	4.3 (0.6)	62	1410.4	7.3 (1.0)	98	2968.8	262.4 (50.2)
27	419.4	1.5 (1.5)	63	1411.7	5.5 (2.2)	99	2978.8	40.2 (100.6)
28	512.3	1.7 (3.3)	64	1430.6	0.4 (1.0)	100	2979.1	228.8 (4.1)
29	535.0	1.3 (1.0)	65	1431.2	19.6 (6.6)	101	3037.0	43.1 (26.7)
30	594.7	5.5 (6.1)	66	1435.6	4.0 (8.9)	102	3037.3	39.3 (15.0)
31	630.9	2.5 (13.4)	67	1437.2	7.3 (5.6)	103	3053.3	51.4 (5.4)
32	703.4	2.2 (0.9)	68	1445.7	15.4 (0.3)	104	3053.4	24.9 (27.7)
33	840.5	1.8 (4.3)	69	1446.7	18.9 (14.0)	105	3055.3	17.6 (12.3)
34	863.5	9.6 (14.0)	70	1448.1	2.8 (2.6)	106	3055.3	77.3 (27.8)
35	915.8	4.8 (3.0)	71	1448.6	9.7 (0.0)	107	3062.5	21.1 (2.0)
36	981.5	25.6 (4.3)	72	1454.0	1.3 (11.9)	108	3062.8	23.8 (26.7)

Table 4
Computed vibrational frequencies (scaled by 0.98), and Raman (IR) intensities for singly charged positive ion of TDAE using B3LYP/6-311++G(d,p). Frequencies are in cm^{-1}, Raman activities are in $Å^4$/amu, and IR activities are in km/mol. The C=C stretch mode (1544 cm^{-1}) is highlighted.

Mode ν_n	Frequency	Raman (IR) activity	Mode ν_n	Frequency	Raman (IR) activity	Mode ν_n	Frequency	Raman (IR) activity
1	64.9	1.2 (0.0)	37	1044.6	0.0 (17.5)	73	1460.2	6.1 (39.7)
2	74.5	0.7 (0.9)	38	1046.7	0.1 (2.2)	74	1462.5	0.9 (29.9)
3	87.9	0.0 (0.8)	39	1047.3	1.2 (12.2)	75	1467.8	42.3 (6.2)
4	117.5	0.2 (1.4)	40	1047.9	1.6 (0.0)	76	1474.9	0.4 (6.5)
5	123.7	0.3 (2.7)	41	1056.1	3.9 (141.8)	77	1475.6	0.0 (16.2)
6	133.5	4.6 (0.0)	42	1094.8	0.0 (12.6)	78	1480.8	59.5 (0.0)
7	142.9	1.7 (2.0)	43	1097.1	0.1 (0.6)	79	1482.3	5.7 (35.4)
8	146.2	0.3 (5.1)	44	1097.1	3.5 (0.0)	80	1486.4	121.8 (0.0)
9	152.5	1.9 (0.0)	45	1098.2	0.2 (0.2)	81	1505.6	3.5 (48.0)
10	172.8	1.8 (0.6)	46	1123.5	0.3 (73.5)	82	1525.1	0.1 (251.9)
11	180.6	1.3 (0.0)	47	1126.8	1.6 (1.3)	83	1535.3	5.1 (49.8)
12	184.0	0.1 (0.4)	48	1133.6	2.2 (0.0)	84	1544.4	59.1 (0.0)
13	187.8	0.2 (0.1)	49	1135.1	0.1 (2.1)	85	2957.7	15.4 (15.4)
14	190.8	0.2 (0.1)	50	1142.7	0.3 (57.5)	86	2957.7	13.9 (12.9)
15	198.8	2.8 (0.0)	51	1155.3	0.2 (2.6)	87	2958.4	60.6 (11.2)
16	219.1	1.0 (0.0)	52	1204.5	17.0 (0.0)	88	2958.7	87.7 (0.0)
17	245.6	0.1 (0.6)	53	1204.9	0.0 (11.7)	89	2960.9	74.6 (13.6)
18	247.6	0.1 (1.1)	54	1219.2	3.3 (31.3)	90	2961.5	64.4 (134.6)
19	262.4	2.2 (4.5)	55	1246.2	0.9 (67.5)	91	2962.4	0.1 (108.3)
20	284.3	0.0 (7.4)	56	1296.3	18.1 (0.0)	92	2964.8	1618.6 (0.0)
21	301.1	0.6 (0.0)	57	1362.5	9.4 (148.5)	93	3003.9	23.9 (42.9)
22	324.1	15.9 (0.0)	58	1396.3	3.7 (31.6)	94	3004.3	117.9 (38.9)
23	335.7	0.4 (1.5)	59	1403.1	0.0 (119.6)	95	3006.4	311.2 (0.0)
24	342.2	0.8 (4.9)	60	1418.0	1.5 (10.8)	96	3006.4	186.6 (30.2)
25	353.2	1.7 (0.4)	61	1419.1	8.4 (0.7)	97	3009.7	16.0 (6.5)
26	407.3	5.7 (0.0)	62	1419.9	9.5 (0.0)	98	3010.3	75.7 (1.9)
27	416.6	1.4 (0.4)	63	1420.9	2.8 (35.6)	99	3010.5	122.8 (0.0)
28	502.4	0.0 (3.6)	64	1441.4	15.8 (0.0)	100	3011.0	4.3 (4.6)
29	538.8	1.2 (1.7)	65	1441.9	1.6 (6.4)	101	3079.8	42.8 (0.0)
30	570.3	7.9 (1.6)	66	1447.1	2.6 (4.2)	102	3079.9	19.5 (0.1)
31	591.6	21.2 (0.0)	67	1450.6	36.8 (0.0)	103	3081.3	37.3 (6.2)
32	665.3	0.8 (1.9)	68	1453.4	22.7 (9.4)	104	3081.4	23.0 (14.0)
33	841.6	0.5 (6.7)	69	1454.4	2.5 (0.5)	105	3083.0	72.6 (8.5)
34	858.3	10.9 (40.5)	70	1457.5	0.6 (14.4)	106	3083.2	5.2 (14.7)
35	902.3	1.9 (11.9)	71	1459.3	10.5 (0.0)	107	3083.2	0.4 (6.0)
36	987.0	15.5 (0.0)	72	1459.9	17.7 (15.7)	108	3083.4	26.4 (0.0)

5.2. Experimental results

TDAE time-of-flight mass spectra from 20 and 40 eV electron ionization are presented in Fig. 3. The parent ion ($C_{10}H_{24}N_4^+$) at 200 amu and many fragment ions in the mass range of 45–185 amu were observed in the mass spectrum. Here, we have attempted to assign each peak to specific fragment ions although further experiments such as MS/MS might be needed to justify these assignments. The major fragment ions include parent–CH_3 (185 amu), parent–$(CH_4)_2$ (168 amu),

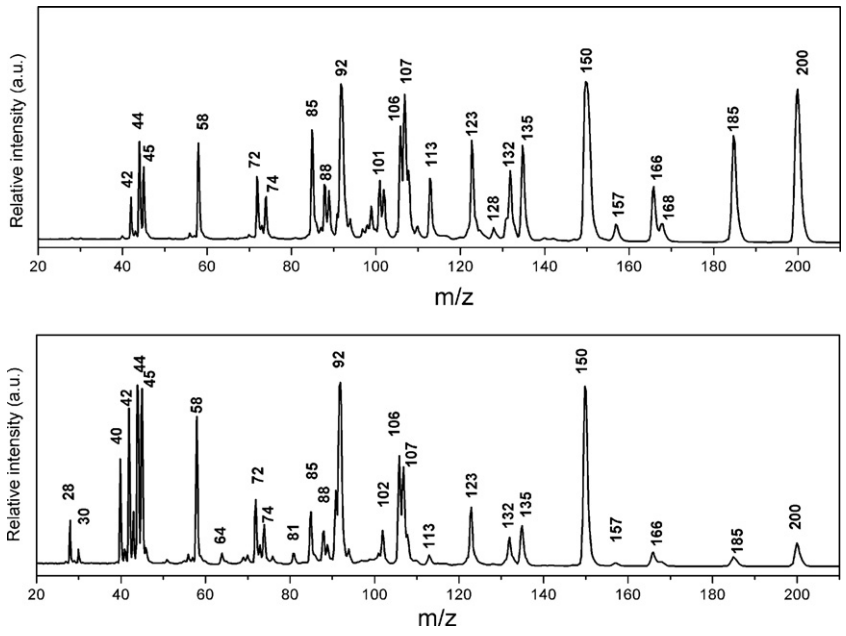

Fig. 3. TOF mass spectra of TDAE with electron energies of 20 eV (top) and 40 eV (bottom).

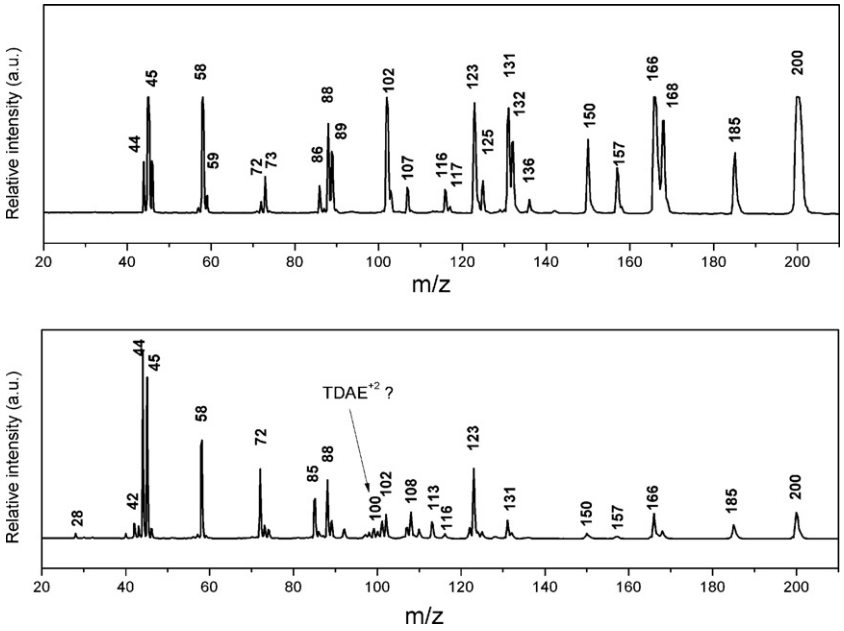

Fig. 4. TOF mass spectra of oxidized-TDAE with electron energies of 20 eV (top) and 40 eV (bottom).

parent–$N(CH_3)CH_2$ (157 amu), parent–$N(CH_3)_2H_6$ (150 amu), parent–$N_2(CH_3)_2H_7$ (135 amu), parent–$N_2(CH_3)_3H_4$ (123 amu), parent–$N_2(CH_3)_3CH_2$ (113 amu), $N_2(CH_3)_4$ (88 amu), $C_3H_9N_2$ (73 amu), C_3H_8N (58 amu), and $NH(CH_3)_2$ (45 amu). At very low energy (~6 eV, not shown here) only the parent ion was present. Fragment ions are observed to be more dominant than that of the parent ion for electron energies above ~40 eV.

It should be noted that in order to obtain these sets of data, extreme care was taken to minimize the reaction of TDAE with oxygen since, as stated before, TDAE is extremely air sensitive. In this regard, in another experiment (Fig. 4), we observed a mass peak at 116 amu, which was not present in the first set of data. We contribute this peak to the reaction of TDAE with oxygen. Oxidation of TDAE may result in dissociation of the central C=C bond [32] to give excited species, which subsequently fluorescence with a bright green color. In this regard, the ion at 116 amu can be assigned to the $C_5H_{12}N_2O^+$ ion as a result of a reaction of TDAE with oxygen. In Fig. 4 (bottom spectrum), we also observe a mass corresponding to $C_5H_{12}N_2{}^+$ (100 amu). The mass 100 amu could also be attributed to the doubly charged ion of TDAE ($TDAE^{2+}$). Yatsuhashi et al. [33] have reported evidence for the existence of doubly charged TDAE previously, though the mass resolution of the accompanying isotopes in this apparatus does not allow us to verify this possibility. However, since this mass was not observed in the not-oxidized TDAE mass spectrum, with the same experimental conditions, we attribute this mass to the $C_5H_{12}N_2{}^+$ ions.

Fig. 5 shows a typical ionization curve of TDAE as a function of electron energy. The argon ion signal, which was used to calibrate the electron energy, is also shown. As seen in Fig. 5, the parent ion onset occurs at ~5.3 eV and peaks at ~20 eV. The cross section steadily decreases above ~20 eV. The energy threshold for the formation of the parent ion was found to be 5.3 ± 0.2 eV.

Fig. 6 shows the photoionization efficiency spectrum of jet-cooled TDAE. The parent ion signal begins at ~5.20 (5) eV, slowly rises to 5.30 (5) eV, and then continues to rise more sharply. These energies were corrected by adding 0.014 eV (110 cm^{-1}) to the laser energy used for the photoionization. This small correction is due to the ionization-threshold shift induced by the DC field (320 V cm^{-1}) used to extract the ions in the time-of-flight mass spectrometer and estimated with the relation $\Delta IP\ (cm^{-1}) = 6.1\,E^{1/2}$, where E is the field strength in units of V cm^{-1}. The slowly rising ion signal in Fig. 6 between 5.20 and 5.30 eV may arise from photoionization of vibrationally excited neutral molecules or poor Franck–Condon factors due to a large geometry difference between the neutral and ionized states. To investigate the origin of the ion signal in this energy region, photoionization efficiency spectra were measured by replacing He with Ar as the carrier gas. If these ions originate from ionization of the vibrationally excited molecules, their relative intensities should decrease with Ar carrier gas. This is because the Ar supersonic beam has a higher cooling efficiency than He, resulting in lower internal temperatures of the neutral molecules and thus smaller populations in the excited levels [34]. However, the photoionization spectra of TDAE seeded in Ar and He show very similar profiles, suggesting that the slowly rising ion signal is not due to ionization of vibrationally excited neutral molecules. On the other hand, our DFT calculations predicted significant geometry differences between the ground electronic states of the neutral and ionized molecules, which should result in poor Franck–Condon (FC) factors for transitions around the band origin. Using the equi-

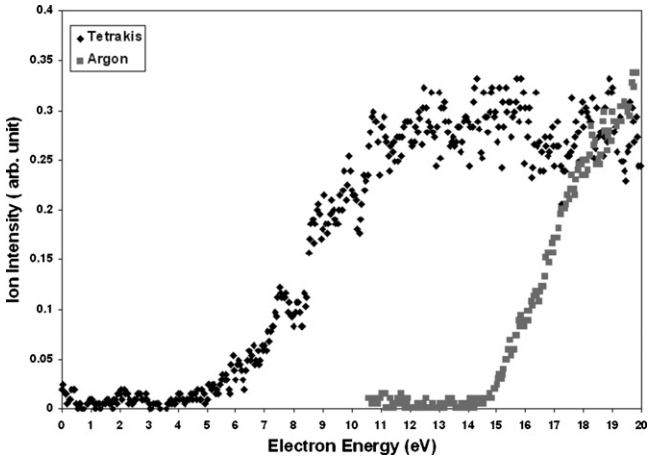

Fig. 5. Ionization potential of parent ion of TDAE ($C_{10}H_{24}N_4{}^+$) compared with that of Ar^+ from the argon seed gas. The TDAE data represents the overlap of a number of spectra.

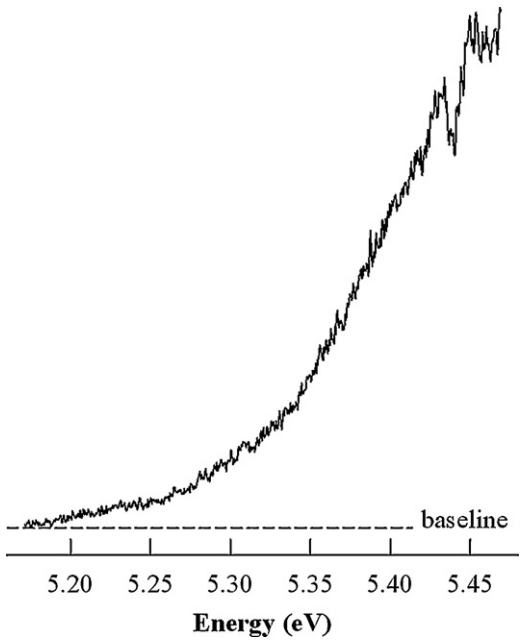

Fig. 6. Photoionization efficiency spectrum of TDAE seeded in helium carrier gas.

librium geometries and vibrational force fields of the neutral and ionized molecules predicted by DFT, we calculated multidimensional FC factors [35]. The FC factor for the 0-0 transition between the vibronic ground states of the neutral and ion molecules is very small ($\sim 10^{-6}$), and significant FC factors ($\sim$5%) begin at $\sim$0.2 eV above the 0-0 transition. Therefore, the first ionization onset at 5.20 (5) eV measured from the photoionization efficiency curve should correspond to the upper bound of the adiabatic IP of TDAE.

Fig. 7 compares the calculated and observed Raman vibrational frequencies of TDAE. As it can be seen, the strongest Raman shift in the experimental spectrum is 1632 cm^{-1}. From the calculation, this mode was attributed to the C=C stretch mode. This stretch mode is also in close agreement with the previously reported value (1630 cm^{-1}) [21]. There is also good agreement between most of the experimental and computed frequencies, demonstrating that the D_2 symmetry for TDAE is a reasonable structural symmetry. However, the calculated intensities do not correspond exactly to the experimental values, which is not unusual. The difficulty in predicting the Raman intensities is due to the fact that the Raman intensity is the differentiated frequency-dependent polarizability with respect to nuclear displacements and such a calculation demands a very high-level computational method with the inclusion of sufficiently large basis sets in the wave function describing the molecule.

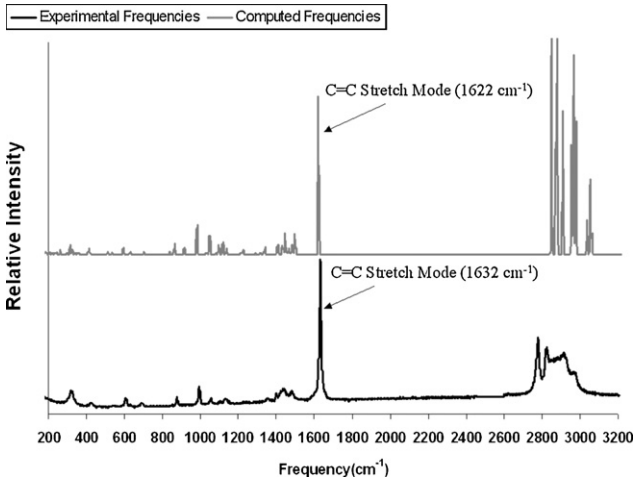

Fig. 7. Comparison between calculated (top) and experimental (bottom) Raman spectra of TDAE. The experimental data were recorded with Ar laser at room temperature (20 °C).

The intense C=C Raman mode has no accompanying IR activity (obtained from the calculation) and adds confidence that TDAE possesses a centro-symmetric structure (mutual exclusion principle). As discussed in the computational section, this mode is expected to shift to 1544 cm^{-1} upon ionization of TDAE.

Thus far, in our discussion we have focused on the optimized structure of TDAE and its properties. However, it is important to consider the relative energies for the isomers of TDAE. Fleurat-Lessard and Volatron [36] have extensively studied different geometries resulting from pyramidalization or rotational isomers of the amino groups in TDAE. In their paper, they concluded that TDAE only has two minima as a result of strong steric effects. The energy difference between the two minima was found to be 0.026 eV (MP2/HF calculation level). It is thus very likely that in our experiments we have both isomers. We also computed the difference in energy between these two isomers using the B3LYP/6-311++G** basis set and also obtained a value of 0.02 eV.

We performed further Raman studies of TDAE in search of evidence for these isomers (lowest energy = conformer I, 0.026 eV higher in energy = conformer II) at two extreme temperatures: room (295 K) and liquid nitrogen (77 K) temperatures. Raman spectra for TDAE at room temperature and under liquid nitrogen (RUN) are presented in Fig. 8. As seen in Fig. 8, the RUN spectrum exhibits very similar band positions as the room temperature spectrum. However the relative band intensities at the two temperatures vary considerably. The C=C stretching frequency (1632 cm^{-1}) remains the most intense line at the two temperatures. Raman under liquid nitrogen (RUN) usually shows much higher spectral resolution as a result of ro-vibrational cooling [29]. Accordingly, the two bands in the 1100 cm^{-1} region become better resolved in the RUN spectrum. The main conclusion is that the same Raman transitions are observed at room temperature and with liquid nitrogen cooling. In many cases where two different isomers are present, the highest energy isomer will be absent at 77 K (e.g., only the trans isomer is present in RUN for cis/trans 1,2-dichloroethane), however for TDAE, we did not observe changes in the Raman transition bands for the two different temperatures.

In Fig. 8, we compare the calculated Raman frequencies and intensities for the two different isomers. Although it is difficult to draw much conclusion from this figure, it is interesting to focus on the two bands at 865 and 938 cm^{-1}. These two bands have almost the same intensity for the lowest energy structure (conformer I). For conformer II (0.02 eV higher in energy), 938 cm^{-1} band is stronger than the 865 cm^{-1} band. In the experimental spectra, we observe that these two bands (865 and 938 cm^{-1}) have the same intensity in the case of RUN experiment. The same trend is observed for 2600–300 cm^{-1} bands. These bands have almost the same intensity as shown in Fig. 9. A glance at Fig. 8 shows that these bands have the same intensity in the RUN spectrum. These observations suggest that upon reducing the temperature of the sample from room to liquid nitrogen, the Raman lines better reflect the frequencies and intensities of the lowest energy structure (conformer I). Finally the *drastic* reduction of the main feature (1632 cm^{-1}) relative to the other lines in the RUN spectrum is not understood unless it is related to the decrease in conformer II. We also observed that the intensities of the other frequencies decrease in the RUN spectrum especially in the higher frequencies (2800–300 cm^{-1}). In conclusion, although our Raman experiments suggest that at lower temperature the Raman lines better reflect the frequencies and intensities of the lowest energy structure, higher energy conformer

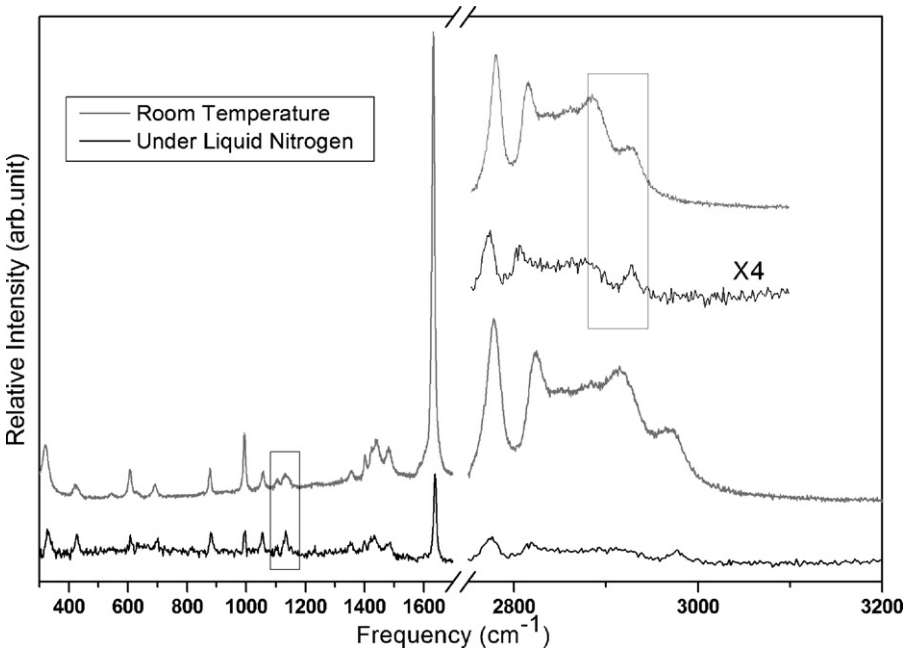

Fig. 8. Comparison between Raman spectra for TDAE at room temperature and under liquid nitrogen (RUN).

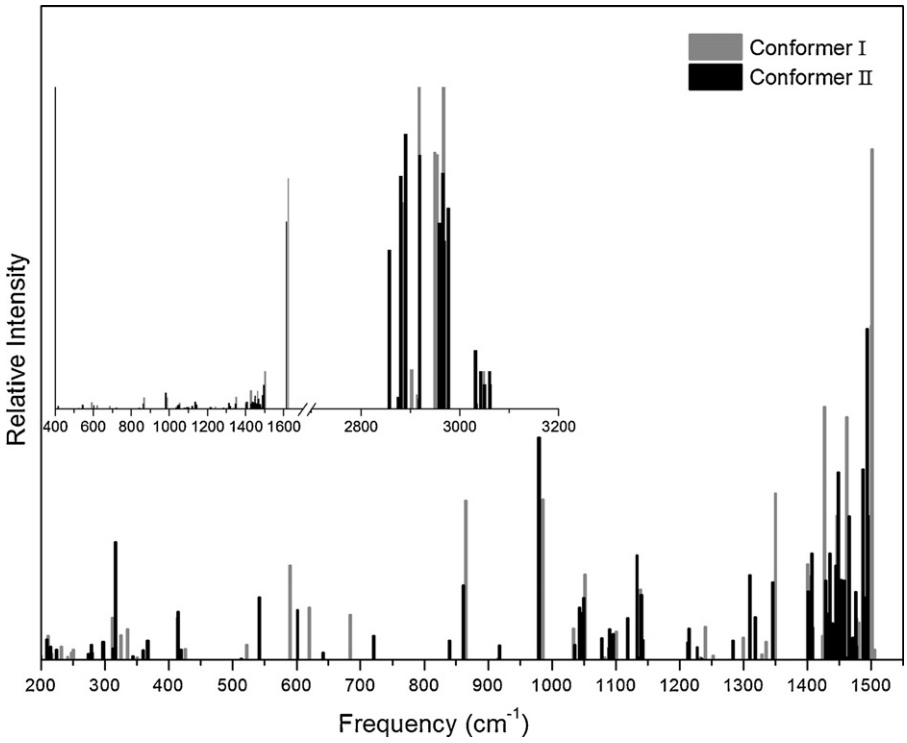

Fig. 9. Comparison between Raman intensities for conformer I (lowest energy) and conformer II (0.02 eV higher in energy) of TDAE computed using B3LYP/6-311++G(d,p).

(conformer II) could still exist under liquid nitrogen conditions, i.e., no transition bands disappear the RUN spectrum. However, provided that the energy difference of the two lower conformers is about 0.02 eV, the sample should be predominantly in its lowest energy state.

6. Conclusion

In summary, we report refined IP values of jet-cooled TDAE obtained from electron ionization and laser ionization spectroscopy. The upper limits of the adiabatic IP are measured to be 5.3 ± 0.2 eV from electron impact ionization and 5.20 ± 0.05 eV from laser photoionization. The DFT calculations show that although the bond distances are changed upon ionization, the conformation of TDAE appears to be unaltered. The bond-length changes may be attributed to the 0.6 eV difference between the adiabatic and vertical ionization potentials. In addition, we measured a C=C stretching frequency of TDAE using laser Raman spectroscopy and compared it with the computed value. Good agreements between the experimental and computational frequencies were observed, which provided further validation for the predicted structure of TDAE. Finally, this work provides a better

understanding of the properties of the low-IP TDAE compound and may offer useful insights for designing and synthesizing other low-IP organic compounds.

Acknowledgement

Funding for this research is provided by the National Science Foundation (Grant No. CHE-0848487 for RNC and CHE-1012351 for DSY). One of the authors (N.M.) would like to thank Dr. C. Feigerle with the Raman experiment.

References

[1] Y. Nakato, M. Ozaki, A. Egawa, H. Tsubomura, Chem. Phys. Lett. 9 (1971) 615–616.
[2] J.R. Woodworth, T.A. Green, C.A. Frost, J. Appl. Phys. 57 (1985) 1648–1655.
[3] Y.S. Zhang, J.E. Scharer, J. Appl. Phys. 73 (1993) 4779–4784.
[4] K.L. Kelly, J.E. Scharer, E.S. Paller, G. Ding, J. Appl. Phys. 92 (2002) 698–709.
[5] J. Seguinot, T. Ypsilantis, Nucl. Instrum. Meth. 142 (1977) 377–391.
[6] J. Seguinot, T. Ypsilantis, Nucl. Instrum. Meth. Phys. Res. A 343 (1994) 1–29.
[7] D.F. Anderson, IEEE Trans. Nucl. Sci. 28 (1981) 842–848.
[8] P.M. Allemand, K.C. Khemani, A. Koch, F. Wudl, K. Holczer, S. Donovan, G. Grüner, J.D. Thompson, Science 253 (1991) 301–302.
[9] K. Tanaka, A.A. Zakhidov, K. Yoshizawa, K. Okahara, T. Yamabe, K. Yukushi, Phys. Rev. B 47 (1993) 7554–7559.
[10] L. Lindell, M. Unge, W. Osikowicz, S. Stafström, W. Salaneck, X. Crispin, M. de Jong, Appl. Phys. Lett. 92 (2008) 163302 (3 pages).
[11] J.B. Fenn, M. Mann, C.K. Meng, S.F. Wong, C.M. Whitehouse, Science 246 (1989) 64–71.
[12] O. Hampe, M. Neumaier, M.N. Blom, M.M. Kappes, Chem. Phys. Lett. 354 (2002) 303–309.
[13] I.N. Ioffe, S.M. Avdoshenko, O.V. Boltalina, L.N. Sidorov, K. Berndt, J.M. Weber, Int. J. Mass Spectrom. 243 (2005) 223–230.
[14] R.L. Pruett, J.T. Barr, K.E. Rapp, C.T. Bahner, J.D. Gibson, R.H. Lafferty, J. Am. Chem. Soc. 72 (1950) 3646–3650.
[15] H. Weingarten, W.E. White, J. Am. Chem. Soc. 88 (1966) 2885 (1 page).
[16] H. Brederick, F. Effenberger, T. Brendle, Angew. Chem. 78 (1966) 147.
[17] N. Wiberg, Angew. Chem. Int. Ed. 7 (1968) 766–779.
[18] B. Centinkaya, G.H. King, S.S. Krishnamurthy, M.F. Lappert, J.B. Pedley, Chem. Commun. (1971) 1370–1371.
[19] J.M.L. Martin, A. Warshawsky, A. Breskin, R. Chechik, Chem. Phys. Lett. 279 (1997) 389–395.
[20] M.R. Pederson, N. Laouini, J. Cluster Sci. 10 (1999) 557–571.
[21] H. Bock, H. Borrmann, Z. Havlas, H. Oberhammer, K. Ruppert, A. Simon, Angew. Chem. Int. Ed. Engl. 30 (1991) 1678–1681.
[22] N. Wiberg, D.R. Downing, D.D. Coffman, J. Am. Chem. Soc. 87 (1965) 2054–2055.
[23] N. Wiberg, J.W. Buchler, Z. Naturforsch. 19b (1964) 5.
[24] W.D. Robertson, N.I. Hammer, J.E. Bartmess, R.N. Compton, K. Diri, K.D. Jordan, J. Chem. Phys. 122 (2005) 204319.
[25] For a review see N. Mirsaleh-Kohan, W.D. Robertson, R.N. Compton, Mass Spectrom. Rev. 27 (2008) 237–285 and references therein.
[26] W.E. Barr, W.A. Perkins, Rev. Sci. Instrum. 37 (1966) 1354–1359.
[27] W.C. Wiley, I.H. McLaren, Rev. Sci. Instrum. 26 (1955) 1150–1157.
[28] G.K. Rothschopf, J.S. Perkins, S. Li, D.-S. Yang, J. Phys. Chem. A 104 (2000) 8178–8182.
[29] J.S. Hager, J. Zahardis, R.M. Pagni, R.N. Compton, J. Li, J. Chem. Phys. 120 (2004) 2708–2718.
[30] M.J. Frisch, G.W. Trucks, H.B. Schlegel, G.E. Scuseria, M.A. Robb, J.R. Cheeseman, J.A. Montgomery Jr., T. Vreven, K.N. Kudin, J.C. Burant, J.M. Millam, S.S. Iyengar, J. Tomasi, V. Barone, B. Mennucci, M. Cossi, G. Scalmani, N. Rega, G.A. Petersson, H. Nakatsuji, M. Hada, M. Ehara, K. Toyota, R. Fukuda, J. Hasegawa, M. Ishida, T. Nakajima, Y. Honda, O. Kitao, H. Nakai, M. Klene, X. Li, J.E. Knox, H.P. Hratchian, J.B. Cross, V. Bakken, C. Adamo, J. Jaramillo, R. Gomperts, R.E. Stratmann, O. Yazyev, A.J. Austin, R. Cammi, C. Pomelli, J.W. Ochterski, P.Y. Ayala, K. Morokuma, G.A. Voth, P. Salvador, J.J. Dannenberg, V.G. Zakrzewski, S. Dapprich, A.D. Daniels, M.C. Strain, O. Farkas, D.K. Malick, A.D. Rabuck, K. Raghavachari, J.B. Foresman, J.V. Ortiz, Q. Cui, A.G. Baboul, S. Clifford, J. Cioslowski, B.B. Stefanov, G. Liu, A. Liashenko, P. Piskorz, I. Komaromi, R.L. Martin, D.J. Fox, T. Keith, M.A. Al-Laham, C.Y. Peng, A. Nanayakkara, M. Challacombe, P.M.W. Gill, B. Johnson, W. Chen, M.W. Wong, C. Gonzalez, J.A. Pople, GAUSSIAN 03, Revision C.02, Gaussian, Inc., Wallingford, CT, 2004.
[31] M.P. Andersson, P. Uvdal, J. Phys. Chem. A 109 (2005) 2937–2941.
[32] C.-C. Huang, K.L. Hohn, J. Phys. Chem. B 114 (2010) 2685–2694.
[33] T. Yatsuhashi, T. Obayashi, M. Tanaka, M. Murakami, N. Nakashima, J. Phys. Chem. A 110 (2006) 7763–7771.
[34] J.F. Fuller, S. Li, B.R. Sohnlein, G.K. Rothschopf, D.-S. Yang, Chem. Phys. Lett. 366 (2002) 141–146.
[35] D.-S. Yang, M.Z. Zgierski, D.M. Rayner, P.A. Hackett, A. Martinez, D.R. Salahub, P.-N. Roy, T. Carrington Jr., J. Chem. Phys. 103 (1995) 5335–5342.
[36] P. Fleurat-Lessard, F. Volatron, J. Phys. Chem. A 102 (1998) 10151–10158.